Hydrogen bonding in water under extreme confinement unveiled by nanoscale vibrational spectroscopy and simulations

*Xintong Xu[†1], Xin Jin[†2,3], Matthias Kuehne[4], De-Liang Bao[2], Joel Martis[1], Yu-Ming Tu[4], Cody L. Ritt[4], Juan Carlos Idrobo[5], Michael S. Strano[4], Arun Majumdar[*1,6,7], Sokrates T. Pantelides[*2,8], Jordan A. Hachtel[*9]*
[†]Equally Contributing First Authors

[1]Department of Mechanical Engineering, Stanford University, Stanford, CA, USA
[2]Department of Physics and Astronomy, Vanderbilt University, Nashville, TN, USA
[3]University of the Chinese Academy of Sciences, Beijing 100049, China
[4]Department of Chemical Engineering, Massachusetts Institute of Technology, MA, USA
[5]Materials Science & Engineering, University of Washington, Seattle, WA, USA
[6]Precourt Institute for Energy, Stanford University, Stanford, CA, USA
[7]Department of Photon Science, SLAC National Laboratory, Menlo Park, CA, USA
[8]Department of Electrical and Computer Engineering, Vanderbilt University, Nashville, TN, USA
[9]Center for Nanophase Materials Sciences, Oak Ridge National Laboratory, Oak Ridge, TN, USA
[*]Correspondence to: arunava@stanford.edu
[*]Correspondence to: pantelides@vanderbilt.edu
[*]Correspondence to: hachtelja@ornl.gov

Fluids under extreme confinement exhibit distinctly new properties compared to their bulk analogs[1–5]. Understanding the structure and intermolecular bonding of confined water lays the foundation for creating and improving applications at the water-energy nexus[6–8]. However, probing confined water experimentally at the length scale of intermolecular and surface forces has remained a challenge. Here, we report a combined experiment/theory framework to reveal changes in H-bonding environment and the underlying molecular structure of confined water inside individual carbon nanotubes. H-bonding is directly probed through the O-H stretch frequency with vibrational electron energy-loss spectroscopy and compared to spectra from molecular-dynamics simulations based on density-functional-theory. Experimental spectra show that water in larger carbon nanotubes exhibit the bonded O-H vibrations of bulk water, but at smaller diameters, the frequency blueshifts to near the 'free' O-H stretch found in water vapor and hydrophobic surfaces. The matching simulations reveal that, in addition to steric confinement, the tube's vibrations play a key role in breaking up the H-bond network, resulting in an orientationally-dispersed, non-H-bonded phase. Furthermore, the temperature-dependence of the vibrations is investigated, providing insights into phase transitions and the confined-water density. This

Exploring Charge Transport Dynamics in a Cryogenic P-Type Germanium Detector

P. Acharya,[1] M. Fritts,[2] D.-M. Mei,[1,*] G.-J. Wang,[1] R. Mahapatra,[3] and M. Platt[3]

[1] *Department of Physics, The University of South Dakota, Vermillion, SD 57069, USA*
[2] *School of Physics and Astronomy, University of Minnesota, Minneapolis, MN, 55455, USA*
[3] *Department of Physics & Astronomy, Texas A & M University, College Station, TX 77843, USA*

(Dated: February 29, 2024)

This study explores the dynamics of charge transport within a cryogenic P-type Ge particle detector, fabricated from a crystal cultivated at the University of South Dakota (USD). By subjecting the detector to cryogenic temperatures and an Am-241 source, we observe evolving charge dynamics and the emergence of cluster dipole states, leading to the impact ionization process at 40 mK. Our analysis focuses on crucial parameters: the zero-field cross-section of cluster dipole states and the binding energy of these states. For the Ge detector in our investigation, the zero-field cross-section of cluster dipole states is determined to be $8.45 \times 10^{-11} \pm 4.22 \times 10^{-12}$ cm^2. Examination of the binding energy associated with cluster dipole states, formed by charge trapping onto dipole states during the freeze-out process, reveals a value of 0.034 ± 0.0017 meV. These findings shed light on the intricate charge states influenced by the interplay of temperature and electric field, with potential implications for the sensitivity in detecting low-mass dark matter.

I. INTRODUCTION

Recent astronomical investigations consistently highlight the pivotal role of dark matter (DM) in the cosmos, characterized by its non-luminous and non-baryonic nature, constituting the majority of the universe's material composition [1–4]. Strong evidence supports the notion that DM influences the cosmos by creating expansive halos around galaxies, as observed in the Milky Way [5–8]. The quest for direct evidence lies within laboratory research, exploring potential interactions between DM particles and ordinary matter beyond gravitational forces. While weakly interacting massive particles (WIMPs) have been a focus, recent theoretical frameworks like asymmetric DM and dark sectors prompt exploration of low-mass DM particles. Thus, the MeV-scale particle emerges as a noteworthy candidate for low-mass DM [9–11], yet detecting them poses challenges. The need for detectors with exceptional sensitivity to discern a solitary electron-hole (e-h) pair complicates matters due to the narrow energy span involved. Overcoming this hurdle requires leveraging modern technology and innovative methodologies for precise and reliable capture and quantification of these minute energy signals. The relentless pursuit of sophisticated detectors and pioneering detection techniques continues as researchers delve deeper into the mysteries surrounding low-mass DM [12]. These advancements hold the promise of unraveling one of the universe's profound enigmas, potentially bringing us closer to understanding its intricate tapestry.

Owing to their exceptional sensitivity, germanium (Ge) detectors have emerged as a promising avenue for addressing the challenge of low-mass DM detection, presenting a compelling alternative to conventional methodologies [13]. These detectors possess a distinct advantage for probing low-mass DM due to their remarkable ability to efficiently generate electron-hole pairs, each requiring an average energy of 3 eV. Complementing this characteristic is Ge's narrow band gap of ∼0.7 eV, further bolstering its suitability for such investigations at millikelvin (mK) temperatures [14]. Leveraging the concept of doping, it becomes possible to significantly expand the parameter space for detecting low-mass DM using Ge detectors. By judiciously introducing impurities into the Ge matrix, particularly shallow-level impurities boasting binding energies around 0.01 eV, a fascinating phenomenon emerges: the creation of dipole states and cluster dipole states in conditions below 6.5 K [15]. What distinguishes these dipole states and cluster dipole states is their binding energy, which plunges even lower than that of the impurities themselves [16, 17]. This intriguing aspect opens a pathway to potentially detecting low-mass DM.

Yet, despite well-explored knowledge concerning the binding energies of impurities in Ge, a conspicuous gap remains regarding the binding energies of these dipole states and cluster dipole states at cryogenic temperatures, especially those hovering below 100 mK. When Ge is cooled to these frigid temperatures, as experienced in the vicinity of liquid helium, a compelling process unfolds: the expulsion of residual impurities from its conduction or valence bands. These expelled impurities then find solace in localized states, giving rise to electric dipoles (denoted as D^{0^*} for donors and A^{0^*} for acceptors) or neutral states (D^0 and A^0). These states signify excited neutral impurity configurations, tethered by binding energies less than 10 meV. The captivating implication here is the capacity of these dipole states to ensnare charge, thereby orchestrating the formation of cluster dipole states (D^+ and D^- for donors, and A^+ and A^- for acceptors), which exhibit even lower binding energy levels. The specifics of these states depend on the operational temperature [15, 18, 19].

* Corresponding author.
Email: Dongming.Mei@usd.edu

A Tampering Risk of Fiber-Based Frequency Synchronization Networks and Its Countermeasures

Hongfei Dai, Yufeng Chen, Wenlin Li, Fangmin Wang, Guan Wang, Zhongwang Pang, and Bo Wang

***Abstract*—Fiber optic networks are used worldwide and have been regarded as excellent media for transmitting time-frequency (TF) signals. In the past decades, fiber-based TF synchronization techniques have been extensively studied. Instruments based on these techniques have been successfully applied. With the increasing application of TF synchronization instruments, their security has become an important issue. Unfortunately, the security risks of fiber-based frequency synchronization (FbFS) instruments have been overlooked. This paper proposes a frequency tampering method called "frequency lens". On a 200 km fiber link, we demonstrate a frequency tampering scenario using a frequency lens-enabled frequency tampering module (FTM). On the user side, the frequency value of the recovered 100 MHz signal can be stealthily altered within a range of 100 MHz±100 Hz, while the frequency dissemination stability of the system remains normal. Related to this tampering risk, potential hazards in three different application scenarios, which rely on precise frequency references, are analyzed. Two countermeasures are also proposed to solve this tampering risk.**

***Index Terms*—Fiber-based frequency synchronization; fiber network; tampering risk.**

I. Introduction

At present, optical fiber networks are used worldwide and have been one of the largest infrastructures for human utilization. As an excellent transmission medium, the optical fiber has unique advantages in transmitting time-frequency (TF) reference. In the past decades, fiber-based TF synchronization techniques have been widely studied [1]–[10]. The related instruments have been successfully applied in various fields, such as metrology [6], [8], [11], communication [12], navigation [13], and radio astronomy [14], [15], as shown in Fig. 1. In the near future, fiber-based TF synchronization instruments will support strict timing requirements in the fields of fifth-generation/sixth-generation communication [16], smart cities [17], global seismic monitoring [18], [19], and distributed computation [20].

With the increasing applications of fiber-based TF synchronization instruments, their security has become an important issue that must be considered in advance [21]. There have been previous studies on attacks and countermeasures related to fiber-based time synchronization (FbTS) systems [22]–[26]. However, research on corresponding aspects of fiber-based frequency synchronization (FbFS) systems is limited. Notably, those methods designed for attacking FbTS cannot be directly applied to FbFS. The primary method in attacking FbTS is to partially disrupt the symmetry of the fiber link in both forward and backward directions, causing asymmetry in the delay of time signals within the link. However, the asymmetry of a small portion of the fiber link cannot cause a disastrous effect on frequency synchronization. For FbFS instruments, the disastrous attack is covertly and slightly tampering with the disseminated frequency reference without affecting its stability. This means that third parties can control important applications with a frequency tampering module (FTM), as shown in Fig. 1. It would not disrupt the normal operation of applications relying on frequency synchronization but could lead to incorrect or biased results.

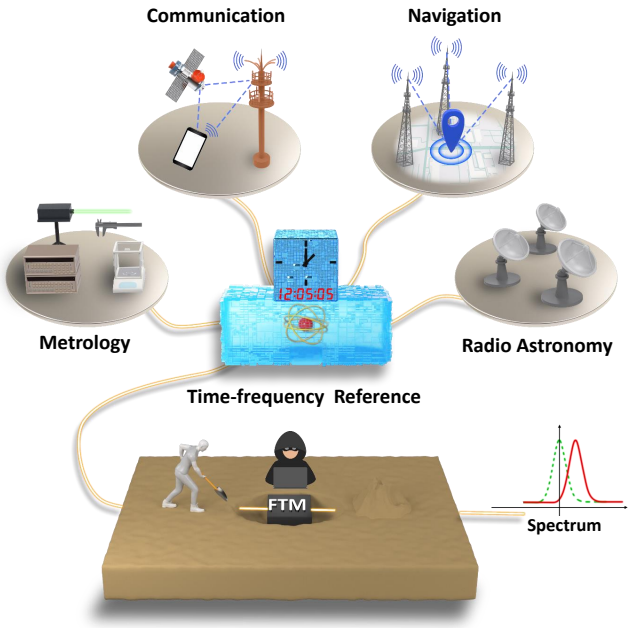

Fig. 1. Schematic diagram of the fiber-based TF synchronization network and tampering risk behavior. FTM, frequency tampering module.

For FbFS systems, there are normally two phase-locked loops (PLLs), as shown in Fig. 2(a). PLL1 is used to compensate for the phase fluctuation induced by fiber dissemination. PLL2 is used as a clean oscillator to optimize the phase noise spectrum of the recovered frequency signal [4], [27]. Monitoring the locking status of PLL1 normally serves as an effective method for system security monitoring. PLL1

This work was supported in part by the National Natural Science Foundation of China under Grant 62171249, in part by the National Key Project of Research and Development under Grant 2021YFA1402102, and in part by Tsinghua Initiative Scientific Research Program. *(Corresponding author: Bo Wang.)*

The authors are with State Key Laboratory of Precision Space-time Information Sensing Technology, Department of Precision Instrument, Tsinghua University, Beijing 100084, China, and also with the Key Laboratory of Photonic Control Technology (Tsinghua University), Ministry of Education, Beijing 100084, China (e-mail: bo.wang@tsinghua.edu.cn).

A Compact Anomaly Detection Solution for Science Instruments

Alfonso Lagares de Toledo
School of Aerospace Engineering
Georgia Institute of Technology
Atlanta, GA 30312
alagares@gatech.edu

Christopher E. Carr
School of Aerospace Engineering &
School of Earth and Atm. Sciences
620 Cherry St NW, Room G10
Atlanta, GA 30312
cecarr@gatech.edu

Abstract*—Small, low-cost instruments enable new and exciting mission opportunities, yet their constrained volume and limited budgets make them especially susceptible to suffering anomalies during flight. Radiation effects, as well as sensor or actuator failure, can all pose a serious threat to the continued collection of scientific data as well as cause the partial or complete loss of a mission's science payload. Onboard anomaly detection could allow instruments to recover from such events, but its ad-hoc development typically falls outside the mission's timeline or monetary constraints. Here we describe a compact solution for the implementation of onboard anomaly detection meant for space science missions. The device is designed to be interoperable with a broad range of instruments, utilizing easily accessible power and logic signals to monitor the state of peripherals and actuators without disrupting their functionality. By leveraging a commercially-available microcontroller with a radiation-hardened alternative package, the device can be inexpensively sourced and assembled with minimal work, enabling instrument characterization on an expedited timeline. The system can then be exchanged for a radiation-hardened version, ensuring the replicability of observed anomalies in a laboratory environment during instrument operations. We also present currently implemented anomaly detection algorithms, which enable the system to detect anomalies in instruments with varying failure modes and allow mission designers to choose which detection approach best fits the specific needs of their instrument. Finally, we showcase an example application of this system in the detection of anomalies during the operation of a lysis motor designed for use in biological space instruments. The inclusion of the described anomaly detection system into new or existing instruments can effectively lower the risks associated with in-flight anomalies, improving their reliability while causing minimal impact on their development timeline or system complexity. This newfound capability can be leveraged to improve the resilience of existing science missions or to enable new missions to harsher space environments where anomaly detection is a requirement for successful instrument operation.

TABLE OF CONTENTS

1. INTRODUCTION

Small instruments are rapidly expanding our ability to achieve science objectives with reduced budgets and constrained timelines. This creates exciting opportunities to pursue new mission concepts that were previously not achievable, where mass, volume, or cost constraints limit the use of larger instruments. Missions concepts similar to the Europa Lander [1], the Enceladus Orbilander Mission [2], or the Vertical Entry Robot for Navigating Europa (VERNE) [3] rely on small instruments to achieve their mission goals. Furthermore, instruments that are not yet implemented in specific mission architectures, like the ELIE [4] or SETG [5] instruments, have the potential to improve or enable new measurements and observations to answer still unanswered questions in planetary science. Small science missions are an integral part of current and future strategies to advance in-situ investigation of planetary or small-body environments, as they provide a valuable combination of launch cadence, complexity, and risk that enables them to respond to ongoing scientific development [6].

However, these instruments pose unique implementation challenges for mission designers, one of which is reliable anomaly detection that can adapt to the requirements of these instruments. During the course of a mission, instruments will encounter anomalies that can threaten their successful operation, the collection of data, and the achievement of scientific goals. An anomaly is an external or internal event that changes the state or configuration of an instrument to one that can cause temporary or permanent damage to the instrument, or under which the instrument was not designed to operate. Anomalies pose a risk to all spacecraft, but their impact on small missions can be severely detrimental: Between the years 2000 and 2016, 35 percent of small missions failed to meet their objectives [7]. Detecting an anomaly is vital to allow the instrument or spacecraft to respond to it, mitigating its disruption to ongoing operations and ensuring the safety and continuity of the mission.

The need for anomaly detection can be driven by multiple mission requirements. Recovery from anomalies into a functional or safe state can be a requirement for missions where the occurrence of an anomaly threatens the continuation of the mission or the achievement of its mission goals unless corrective action is taken. It can also be a requirement for instruments where the medium to sample is a-priori unknown. Detecting an anomaly in the instrument's operation can indicate the presence of an unfamiliar sample medium, allowing mission controllers to halt operations and conduct further studies before the instrument proceeds with sample analysis, thus mitigating the risk of damage to the instrument. A requirement for increased reliability can also drive the need for anomaly detection capabilities. Resource restrictions drive instrument designers to use commercial-of-the-shelf (COTS) or low technology readiness level (TRL) technologies in instrument designs which increases the risk of anomalies

All-heavy pentaquarks in a nonrelativistic potential quark model

Zhi-Biao Liang[1], Feng-Xiao Liu[2,3] *, and Xian-Hui Zhong[1,3] †

1) Department of Physics, Hunan Normal University, and Key Laboratory of Low-Dimensional Quantum Structures and Quantum Control of Ministry of Education, Changsha 410081, China

2) Institute of High Energy Physics, Chinese Academy of Sciences, Beijing 100049, China and

3) Synergetic Innovation Center for Quantum Effects and Applications (SICQEA), Hunan Normal University, Changsha 410081, China

In a nonrelativistic potential quark model framework, we carry out a serious calculation of the all-heavy pentaquarks by adopting the explicitly correlated Gaussian method. A complete mass spectrum for the $1S$ states is obtained. For the $ccccc\bar{c}$, $cccc\bar{b}$, $bbbbc\bar{c}$, $bbbbb\bar{b}$, $ccbbc\bar{c}$, and $bbccb\bar{b}$ systems, the obtained states are compact and lie far above the lowest dissociation baryon-meson threshold. While, in the $cccbc\bar{c}$, $cccbb\bar{b}$, $bbbcc\bar{c}$, and $bbbcb\bar{b}$ systems with $\{123\}4\bar{5}$ symmetry, the two low-lying configurations with $J^P = 5/2^-$ and $3/2^-$ have a typical molecular structure due to the special role of the color-Coulomb interactions, they may be good candidates of stable states below the dissociation baryon-meson thresholds.

I. INTRODUCTION

Searching for genuine exotic multiquark states beyond the conventional meson ($q\bar{q}$) and baryon (qqq) states has been one of the most important initiatives since the establishment of quark model in 1964 [1–3]. Since the discovery of $X(3872)$ by Belle in 2003 [4], many tetraquark candidates, such as the series hidden-charmed/bottom XYZ states [5], the doubly-charmed state $T_{cc}(3875)^+$ [6, 7], and charmed-strange states [8, 9], have been observed in experiments. Furthermore, the exotic P_c [10–12] and P_{cs} [13] states as candidates of pentaquark states were also reported by the LHCb collaboration. All of these observed exotic states contains two or three light quarks, it is very difficult to determine whether they are hadronic molecular states or genuine multiquark states due to the role of light-meson exchanges. This dilemma should be largely alleviated for the all-heavy multiquarks. They are most likely to be genuine multiquark states since there is no light-meson exchange potential, which is often needed by the formation molecules. Thus, the study of the all-heavy multiquarks may provide an interesting way for establishing the genuine multiquark states.

Impressively, some all-heavy multiquark states have been observed in LHC experiments. In 2020, the LHCb Collaboration observed a narrow structure $X(6900)$ together a broad structure ranging from 6.2 to 6.8 GeV in the di-J/ψ invariant mass spectrum [14]. Later in 2022, the $X(6900)$ was confirmed in the same final state by both the ATLAS [15] and CMS [16] collaborations. Moreover, in the lower mass region the CMS measurements show that a clear resonance $X(6600)$ lies in the di-J/ψ spectrum. These clear structures may be evidences for genuine all-charmed tetraquark $cc\bar{c}\bar{c}$ states. The discovery of $cc\bar{c}\bar{c}$ states has demonstrated the powerful abilities of LHC in productions of fully-heavy hadrons, and also indicates that the all-heavy pentaquark should be exist. Thus, one may expect to observe some all-heavy pentaquarks in forthcoming experiments.

Stimulated by these, some relative studies of the all-heavy pentaquarks have been carried out within various models in recent years. The all-charmed and -bottom pentaquarks were studied with the QCD sum rules [17, 18]. For the baryon-meson type, the masses of $ccccc\bar{c}$ and $bbbbb\bar{b}$ are predicted to be ~ 7.41 GeV and ~ 21.60 GeV, respectively in Ref. [17], which are notably smaller than those of 7.93 ± 0.15 GeV and 23.91 ± 0.15 GeV predicted for the diquark-diquark-antiquark type in Ref. [18]. In Ref. [19], the mass spectra of the $1S$-wave all-heavy pentaquarks were systematically studied with the simple chromomagnetic interaction (CMI) model. The masses of $ccccc\bar{c}$ and $bbbbb\bar{b}$ are predicted to be ~ 7.9 GeV and ~ 23.8 GeV, respectively, which are slightly above the lowest dissociation baryon-meson mass threshold. While, there may exist a stable $J^P = 3/2^-$ $bbccb\bar{b}$ states with a mass of ~ 17.4 MeV. In Ref. [20], the all-heavy pentaquarks were further studied within the MIT bag model by including the chromomagnetic interaction. In this framework, the masses of $ccccc\bar{c}$ and $bbbbb\bar{b}$ are predicted to be ~ 8.2 GeV and ~ 24.8 GeV, and no stable states below the dissociation baryon-meson thresholds are found.

In the recent two years, the all-heavy pentaquarks have been studied with more comprehensive potential quark models, where besides the chromomagnetic interaction, the confining and Coulomb-like potentials are also included in the calculations. In Refs. [21, 22], the authors studied the all-heavy pentaquarks by using the resonating group method (RGM), in which two-cluster approximation is adopted. They obtained one possible stable $J^P = 1/2^-$ $ccccc\bar{c}$ state with a mass of ~ 7.9 GeV, and two possible stable $bbbbb\bar{b}$ states with $J^P = 1/2^-$ and $J^P = 3/2^-$ in the mass range of ~ 23.8 GeV, and several possible stable candidates in the charmed-bottom pentaquarks. In Ref. [23], considering the baryon-meson and diquark-diquark-antiquark configurations, the authors obtained several narrow resonances above 8.0 GeV and 24.0 GeV for the $ccccc\bar{c}$ and $bbbbb\bar{b}$ pentaquarks, respectively, based on the Gaussian expansion method combined with a complex-scaling range approach. Recently, a more serious dynamical calculation beyond the cluster approximation has been carried out by using the variational method with the trial spatial wave function in a simple Gaussian form [24]. No stable pentaquarks states below the dissociation baryon-meson thresholds are found. The masses for the ground $ccccc\bar{c}$ and $bbbbb\bar{b}$ states are predicted

*E-mail: liufx@ihep.ac.cn
†E-mail: zhongxh@hunnu.edu.cn

Next-to-next-to-leading-order QCD corrections to pion electromagnetic form factors

Long-Bin Chen *,[1] Wen Chen †,[2,3] Feng Feng ‡,[4,5] and Yu Jia §[5,6]

[1] School of Physics and Materials Science, Guangzhou University, Guangzhou 510006, China

[2] Institute of Quantum Matter, South China Normal University, Guangzhou 510006, China
[3] Zhejiang Institute of Modern Physics, School of Physics, Zhejiang University, Hangzhou, Zhejiang 310027, China

[4] China University of Mining and Technology, Beijing 100083, China

[5] Institute of High Energy Physics and Theoretical Physics Center for Science Facilities, Chinese Academy of Sciences, Beijing 100049, China

[6] School of Physical Sciences, University of Chinese Academy of Sciences, Beijing 100049, China

(Dated: February 28, 2024)

We investigate the next-to-next-to-leading order (NNLO) QCD radiative corrections to the pion electromagnetic form factor with large momentum transfer. We explicitly verify the validity of the collinear factorization to two-loop order for this observable, and obtain the respective IR-finite two-loop hard-scattering kernel in the closed form. The NNLO QCD correction turns to be positive and significant. Incorporating this new ingredient of correction, we then make a comprehensive comparison between the finest theoretical predictions and numerous pion form factor measurements in both space-like and time-like regions. Our phenomenological analysis provides strong constraint on the second Gegenbauer moment of the pion light-cone distribution amplitude (LCDA) obtained from recent lattice QCD studies.

Introduction. Originally proposed by Yukawa as the strong nuclear force carrier in 1935 [1], subsequently discovered in the cosmic rays in 1947 [2], the π mesons have always occupied the central stage throughout the historic advancement of the strong interaction. As the lightest particles in the hadronic world (hence the highly-relativistic bound systems composed of light quark and gluons), π mesons entail extremely rich QCD dynamics, exemplified by the color confinement and chiral symmetry breaking. Notwithstanding extensive explorations during the past decades, there still remain some great myths about the internal structure of the π mesons.

A classic example of probing the internal structure of the charged pions is the pion electromagnetic (EM) form factor:

$$\langle \pi^+(P')|J^\mu_{\rm em}|\pi^+(P)\rangle = F_\pi(Q^2)(P^\mu + P'^\mu), \qquad (1)$$

with $Q^2 \equiv -(P'-P)^2$. The electromagnetic current defined by $J^\mu_{\rm em} = \sum_f e_f \bar f \gamma^\mu f$, with $e_u = 2/3$ and $e_d = -1/3$ indicating the electric charges of the u and d quarks.

During the past half century, the pion EM form factor has been intensively studied experimentally [3–29]. From the theoretical perspective, the pion EM form factor at small Q^2 can be investigated in chiral perturbation theory [30] and lattice QCD [31–35], from which one can infer the pion charge radius. On the other hand, at large momentum transfer, the $F_\pi(Q^2)$ is expected to be adequately described by perturbative QCD. Within the collinear factorization framework tailored for hard exclusive reactions [36–42] (for a review, see [43]), at the lowest order in $1/Q$, the pion EM form factor can be expressed in the following form:

$$F_\pi(Q^2) = \iint dx\, dy\, \Phi^*_\pi(x,\mu_F) T(x,y,\frac{\mu_R^2}{Q^2},\frac{\mu_F^2}{Q^2})\Phi_\pi(y,\mu_F), \qquad (2)$$

where $T(x,y)$ signifies the perturbatively calculable hard-scattering kernel, and $\Phi_\pi(x,\mu_F)$ represents the nonperturbative yet universal leading-twist pion light-cone distribution amplitude (LCDA), *i.e.*, the probability amplitude of finding the valence u and $\bar d$ quark inside π^+ carrying the fractional momenta x and $\bar x \equiv 1-x$, respectively. The leading-twist pion LCDA assumes the following operator definition:

$$\Phi_\pi(x,\mu_F) = \int \frac{dz^-}{2\pi i} e^{iz^- xP^+} \langle 0|\bar d(0)\gamma^+\gamma_5 \times \mathcal{W}(0,z^-)u(z^-)|\pi^+(P)\rangle, \qquad (3)$$

with $\mathcal{W}$ signifies the light-like gauge link to ensure the gauge invariance. Conducting the UV renormalization for (3), one is led to the celebrated Efremov-Radyushkin-Brodsky-Lepage (ERBL) evolution equation [38, 40]:

$$\frac{d\Phi_\pi(x,\mu_F)}{d\ln\mu_F^2} = \int_0^1 dy\, V(x,y)\,\Phi_\pi(y,\mu_F), \qquad (4)$$

with $V(x,y)$ referring to the perturbatively calculable ERBL kernel.

Eq. (2) is expected to hold to all orders in perturbative expansion. The hard-scattering kernel

*chenlb@gzhu.edu.cn
†chenwenphy@gmail.com
‡f.feng@outlook.com
§jiay@ihep.ac.cn

EUROPEAN ORGANIZATION FOR NUCLEAR RESEARCH (CERN)

CERN-EP-2024-027
2024/02/29

CMS-TOP-22-003

Search for baryon number violation in top quark production and decay using proton-proton collisions at $\sqrt{s} = 13\,\text{TeV}$

The CMS Collaboration*

Abstract

A search is presented for baryon number violating interactions in top quark production and decay. The analysis uses data from proton-proton collisions at a center-of-mass energy of 13 TeV, collected with the CMS detector at the LHC with an integrated luminosity of $138\,\text{fb}^{-1}$. Candidate events are selected by requiring two oppositely-charged leptons (electrons or muons) and exactly one jet identified as originating from a bottom quark. Multivariate discriminants are used to separate the signal from the background. No significant deviation from the standard model prediction is observed. Upper limits are placed on the strength of baryon number violating couplings. For the first time the production of single top quarks via baryon number violating interactions is studied. This allows the search to set the most stringent constraints to date on the branching fraction of the top quark decay to a lepton, an up-type quark (u or c), and a down-type quark (d, s, or b). The results improve the previous bounds by three to six orders of magnitude based on the fermion flavor combination of the baryon number violating interactions.

Submitted to Physical Review Letters

*See Appendix A for the list of collaboration members

Measurement of Proton-Induced Reactions on Lanthanum from 55–200 MeV by Stacked-Foil Activation

Jonathan T. Morrell,[1] Ellen M. O'Brien,[1] Michael Skulski,[2] Andrew S. Voyles,[3] Dmitri G. Medvedev,[2] Veronika Mocko,[1] Lee A. Bernstein,[4,3] and C. Etienne Vermeulen[1]

[1] *Los Alamos National Laboratory, Los Alamos, NM 87545, USA*

[2] *Brookhaven National Laboratory, Upton, NY 11973, USA*

[3] *University of California, Berkeley, Berkeley, CA 94720, USA*

[4] *Lawrence Berkeley National Laboratory, Berkeley, CA 94720, USA*

(Dated: February 29, 2024)

Cerium-134 is an isotope desired for applications as a chemical analogue to the promising therapeutic radionuclide ^{225}Ac, for use in bio-distribution assays as an *in vivo* generator of the short-lived positron-emitting isotope ^{134}La. In the 50–100 MeV energy range relevant to the production of ^{134}Ce by means of high-energy proton bombardment of lanthanum, existing cross section data are discrepant and have gaps at important energies. To address these deficiencies, a series of 17 ^{139}La foils (99.919% natural abundance) were irradiated in two stacked-target experiments: one at the Los Alamos National Laboratory's Isotope Production Facility (IPF) with an incident proton energy of 100 MeV, and a second at Brookhaven National Laboratory's Brookhaven Linac Isotope Producer (BLIP) with an incident proton energy of 200 MeV — a complete energy range spanning approximately 55–200 MeV. Cross sections are reported for 30 products of ^{139}La(p,x) reactions (representing up to 55% of the total non-elastic cross section), in addition to 24 residual products measured in the ^{nat}Cu and ^{nat}Ti foils that were used as proton flux monitors. The measured production cross sections for ^{139}La reactions were compared to literature data as well as default calculations from the nuclear reaction modeling codes TALYS, EMPIRE and ALICE, as well as the TENDL-2023 library. The default calculations typically exhibited poor predictive capability, due to the complexity of multiple interacting physics models in this energy range, and deficiencies in pre-equilibrium reaction modeling. Building upon previous efforts to evaluate proton-induced reactions in this energy range, a parameter adjustment procedure was performed upon the optical model and the two-component exciton model using the TALYS-2.0 code. This resulted in an improvement in ^{139}La(p,x) cross sections for applications including isotope production, over default predictions.

I. INTRODUCTION

Proton accelerators operating in the approximately 10–200 MeV energy range are advantageous for the production of radioisotopes having characteristics of simultaneous high activity and high *specific* activity, *i.e.*, having a high ratio of the desired radionuclide to "cold" (stable) impurities. These characteristics are generally advantageous to the field of nuclear medicine for the creation of radiopharmaceuticals used in the diagnosis and treatment of various diseases, such as cancers. For example, one such radionuclide we are interested in producing is ^{134}Ce, which has applications as a positron-emitting analogue of the therapeutic isotope ^{225}Ac.

Actinium-225 is an alpha-emitting radionuclide that is currently under study for the treatment of various forms of cancer, such as advanced prostate cancer and acute myeloid leukemia [1–3]. With a half-life of 9.9203 (3) days, ^{225}Ac quickly decays to ^{209}Bi through the emission of four 5–8 MeV α particles and two β^- particles, with the longest-lived intermediate decay product being the 3.234 (7) h ^{209}Pb [4–8]. Having a characteristic range of 50–100 µm in human tissue, these emitted alpha particles have a high likelihood of killing cancerous cells while sparing nearby healthy tissue, provided a sufficiently specific cancer-targeting vector. One example of a promising vector is PSMA-617 (prostate-specific membrane antigen), which has shown efficacy (defined as a decrease in prostate-specific antigen, or PSA, serum concentration of $\geq$50%) in 66% of patients afflicted with advanced (metastatic) prostate cancer, according to a recent meta-analysis [9].

An important aspect of treatment planning in targeted radionuclide therapy is the ability to assay the bio-distribution of the injected radiopharmaceutical, typically with clinical positron-emission tomography (PET) scanners [10]. Unfortunately, ^{225}Ac lacks positron emissions in any of its decay products, negating the possibility of performing such scans directly. Instead, the therapeutic targeting vector must be radiolabeled with a positron-emitting chemical analogue of actinium. Recent studies have demonstrated the ability of ^{134}Ce to act as a PET imaging surrogate for drug conjugates in-